Influence of the buffer layer properties on the intensity of Raman scattering of graphene

S. Dyakov, T. Perova, C. Miao, Ya-Hong Xie, S. Cherevkov, A. Baranov

Volume 44, Issue 6, pages 803–809, June 2013

Abstract:
Using a model of oscillating dipoles, we simulate the intensity of the G-band in the Raman signal from structures consisting of graphene, separated by an arbitrary buffer layer from a substrate. It is found that a structure with an optimized buffer layer refractive index and thickness exhibits a Raman signal which is nearly 50 times more intense than that from the same structure with a non-optimized buffer layer. The theoretical simulations are verified by Raman measurements on structures consisting of a layer of graphene on SiO2 and Al2O3 buffer layers. The optical contrast of the single graphene layer is calculated for an arbitrary buffer layer. It was found that both the Raman intensity and optical contrast can be maximized by varying the buffer layer thickness.

Introduction

Graphene has attracted a lot of interest since its discovery in 2004, due to its unique physical properties. In particular, graphene is a two-dimensional semiconductor with a zero-width band gap.[1] Quasi-particles in graphene are mathematically described by the Dirac-type Hamiltonian.[1] The high crystalline quality and high carrier mobility of graphene make it a promising material for future electronic devices.

Monolayer graphene, however, is not always appropriate for use in integrated circuits or interconnects. So-called 'few-layer' graphene (FLG) has more suitable properties for integration in microelectronics. The reason for this is that the band gap for FLG can reach up to 0.2 eV and, therefore, it can form a transparent conductive electrode. It also has lower sheet resistance and is less susceptible to the effects of substrate impurities due to interlayer screening.[2-4] Thus, a thorough knowledge of how the electrical, thermal, mechanical and optical properties evolve from monolayer graphene to graphite will facilitate the development of graphene devices.

Typically, a graphene layer (or layers) are deposited on Cu or another transition metal (Ti, Ni, Pd, Pt and Au) by chemical vapor deposition (CVD)[5-9] or ultra-high vacuum-CVD.[8-10] Next, they are transferred (or exfoliated) onto a thin dielectric layer grown on silicon or another suitable substrate (see, for example, Refs.,[5, 11]). We will refer to the intermediate dielectric layer as a buffer layer for simplicity. Because of their relatively low cost, grain size, good etch-ability and their wide applicability in the semiconductor industry, Ni and Cu have received the most attention as graphene substrate materials.[6-9] Single and

multilayered graphene has been grown successfully on polycrystalline Ni,[6, 7, 9] while large-area graphene has successfully been grown on Cu[8] substrates by CVD.

When investigating graphene, it is important to use a characterization technique which is capable of distinguishing the single graphene layer from thicker flakes as well as to measure the graphene thickness to an accuracy of a few layers of graphene. In addition, the area of single-layer flakes has also to be estimated. One possible technique used to perform these measurements is optical microscopy. The visibility of the graphene layer depends on the properties of the buffer layer, principally on its thickness and refractive index, and these parameters determine the optical contrast. A number of investigations of optical contrast, as well as on the performance of optical microscopy as a function of the wavelength range used to increase the visibility of a single graphene layer, have been published recently.[12-16] Another method which has proven to be a powerful tool for distinguishing graphene monolayer is Raman spectroscopy (see, for example, Ref.[10]). Although the Raman technique is incapable of measuring the thickness of graphene monolayers directly, it enables differentiation of a single layer from the thicker flakes up to a thickness of 10 monolayers. It also distinguishes between monolayers and graphite via the behavior of the vibrational bands of graphene in the regions of 1500–1740 cm−1 and 2500–2900 cm−1 (see Refs.[10, 17-23]). These differences are well described by the intensities, positions and widths of the G-band (at ~ 1582 cm−1), 2D-band (at ~ 2680 cm−1) and high wavenumber peaks (at ~ 1720 and 1730 cm−1) near the G-band of the Raman spectra[10, 17-23] as well as by the recently discovered weak band (N-peak, at ~ 1510 cm−1) from the low wavenumber side of the G-band.[18] In particular, the ratio of the G-band to the Si–Si band (at ~ 520 cm−1), IG/ISi, is suggested as a technique for the estimation of graphene layer/layers thickness.[19] The ratio of I2D/IG represents the intrinsic properties of a given type of graphene and has been used to determine the basic structural and electronic properties of graphene such as optical anisotropy,[24] doping concentration[25-27] and number of layers.[17, 20, 22] When the number of layers increases, the 2D-band broadens and the I2D/IG ratio decreases from ~ 2 for a single layer to ~ 0.5 for a double layer and to 0.3 for a triple layer of graphene.

Using a Raman mapping technique, or Raman imaging, it is possible to measure the size of flakes and to determine the crystalline order of a single graphene layer (or a few layers) at every measured point of the area being mapped. The ability of Raman spectroscopy to investigate single graphene layers is based on the enhancement of the Raman signal from graphene for certain thicknesses of the buffer dielectric layer.[28] This phenomenon is explained by the interference of the probe beam and Raman signal in the layered structure.[28] Thus, from the point of view of Raman intensity, the buffer layer thickness is a very important parameter. In particular, for Raman mapping, it is vital to be able to register a Raman spectrum with a good signal-to-noise ratio in a short period of time;

otherwise, area mapping of graphene flakes may take several hours. Thus, use of a suitable buffer layer is a very important consideration when Raman imaging graphene.

The aim of the present study is to perform a simulation of the Raman intensity and optical contrast of graphene as a function of refractive index and buffer layer thickness at various excitation wavelengths (i.e. 457, 488, 514, 633 and 785 nm) in order to design an optimal buffer layer for simultaneous investigations using optical microscopy and micro-Raman spectroscopy. Finally, we experimentally verify these theoretical results.

Experiment

Graphene was grown on copper (Cu) foil and annealed at 1000 °C for 30 min in a hydrogen environment. CVD of graphene on Cu was carried out at a pressure of 30 Torr under a flow of methane and hydrogen. The deposition temperature was 1000 °C, and the growth time was 30 min. After deposition, the samples were cooled down to room temperature in a hydrogen ambient, note that the total hydrogen pressure was 1 Torr. Then, the graphene layers were transferred onto the SiO2/Si and Al2O3/Si substrates using the polydimethylsiloxane wet etching method. Graphene was transferred onto 90, 165 and 290 nm thick, thermally grown SiO2 and 20 and 70 nm thick Al2O3 deposited by atomic layer deposition (ALD). Figure 1 is a schematic diagram of the samples experimentally investigated in this work.

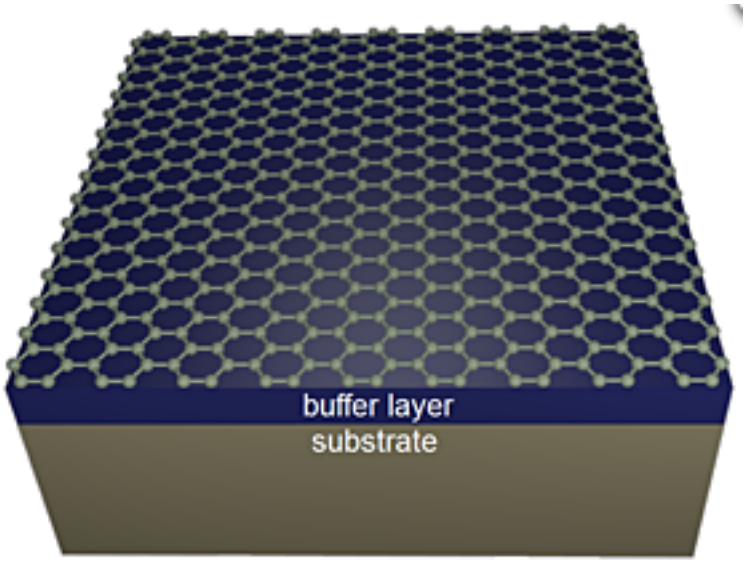

Figure 1. Schematic presentation of the structures investigated with the graphene layer exfoliated onto SiO2/Si or Al2O3/Si substrates.

Raman measurements were carried out in backscattering geometry using a Renishaw 1000 micro-Raman system. An Ar laser at wavelengths of 457, 488 and 514 nm and a HeNe laser at 633 nm at a power of ~ 1–2 mW on the sample were used as excitation sources. The power was kept low to prevent the sample overheating. A semiconductor laser with an excitation wavelength of 785 nm with a power of < 2 mW was also used for Raman measurements of a sample with a 165 nm thick SiO2 layer. A linear dependence of Raman spectrum intensity versus the excitation power was obtained for selected samples in the range of laser power varied from 1 mW to 20 mW, thus excluding a possible influence of stimulated Raman emission on spectra enhancement. The laser spot was focused on the sample surface using 50× and 100× magnification objectives with a short-focus working distance. Up to 8–10 measurements were taken from various points on each sample at each excitation wavelength. Data on the ratio of integrated intensities IG/ISi, discussed in the present paper, were averaged from these measurements.

Modelling

Let us consider a theoretical model describing the intensity of Raman scattering for the layered structure shown in Fig. 1. We select materials for the buffer layers which are commonly used nowadays due to their ease of fabrication on a Si substrate using either chemical or physical vapor deposition or thermal growth.

Spontaneous Raman scattering is a quantum mechanical process with a random spatial distribution of the photons involved; however, the optical behavior of the scattered light can be modeled using classical electromagnetism.[29-33] In order to calculate the Raman intensity from the multilayered samples, we use the optical model reported in Refs.[30, 32] In this model, the ensemble of elementary scatterers is considered to be a system of chaotically oriented oscillating electrical dipoles. The amplitude of oscillation of a dipole is proportional to the electric field strength of the excitation light at the position of a dipole inline image which can be found by the transfer matrix method.[34, 35] The intensity of Raman scattering from the samples is approximated by the intensity of the out-coupled emission of the oscillating dipoles.

The amplitude of the plane wave emitted by dipoles depends on their orientation and polarizations and can be found from the following expressions for vertical dipoles:

$$A_{TE} = 0, \quad A_{TM} = A_0 \sqrt{\frac{3}{8\pi}} \sin \varphi_k,$$

and for horizontal randomly oriented dipoles:

$$A_{TE} = A_0\sqrt{\frac{3}{16\pi}}, \quad A_{TM} = A_0\sqrt{\frac{3}{16\pi}}\cos\varphi_k.$$

Using the boundary conditions for the tangential components of the electric and magnetic field vectors lying immediately on opposite sides of the z0 plane, we obtain the following relationship between vectors of amplitude E of the electromagnetic field:

$$A_{TE} = A_0\sqrt{\frac{3}{16\pi}}, \quad A_{TM} = A_0\sqrt{\frac{3}{16\pi}}\cos\varphi_k.$$

where for vertical dipoles

$$\Delta = A_{TM}\begin{bmatrix}-1\\1\end{bmatrix},$$

for horizontal dipoles

$$\Delta = A_{TE}\begin{bmatrix}-1\\1\end{bmatrix}, \quad \Delta = A_{TM}\begin{bmatrix}-1\\-1\end{bmatrix},$$

and the vector of amplitudes

$$\mathbf{E}(z) \equiv \begin{bmatrix}E^{+}(z)\\E^{-}(z)\end{bmatrix}$$

consists of the amplitudes of plane waves traveling in the positive and negative z-direction. Because we assume that Raman scattering is the only source of radiation, the output vectors of the amplitudes have the form:

$$\mathbf{E}(0-0)=\begin{bmatrix}0\\ E^{-}(0-0)\end{bmatrix},\quad \mathbf{E}(z_N+0)=\begin{bmatrix}E^{+}(z_N+0)\\ 0\end{bmatrix}.$$

The zero components in the 1×2 vectors reflect the fact that there is no incident plane wave either on the top or bottom of the sample. In order to calculate the amplitudes of the positive traveling wave E+(zN + 0) and the negative traveling wave E−(0 − 0), we have to solve the following set of linear algebraic equations:

$$\begin{cases}\mathbf{E}(0)=A\mathbf{E}(z_0-0)\\ \mathbf{E}(z_0-0)=\mathbf{E}(z_0+0)+\Delta.\\ \mathbf{E}(z_0+0)=B\mathbf{E}(h\end{cases}$$

In the set of Eqn (8), the first equation is the relation between the vector of amplitude E(0–0) at the top surface of the sample and that at the z0 − 0 coordinate, the second equation describes the relationship between the vectors of amplitudes E(z0 − 0) and E(z0 + 0) lying immediately on opposite sides of plane z0, and the final equation is the relationship between the vector of amplitudes at z0 + 0 and h + 0 coordinates. From the set of Eqn (8), it follows that

$$E^{-}(0)=(A\Delta)_2-(A\Delta)_1\cdot\frac{(AB)_{21}}{(AB)_{11}},$$

where the expression Xij denotes the ij-element of a matrix X. A scattering layer in the layered structure can be approximated by N planes of oscillating dipoles. In this case, we have to calculate the amplitudes inline image (i = 1, 2, …, N) for each layer independently and the intensity of the output light will be given by †

$$I = \sum_{i=1}^{N} \left| E_i^{-}(0) \right|^2 .$$

Each layer in the model structure in Fig. 1 is considered to be a homogeneous isotropic layer with a refractive index, n, and a thickness, h. The graphene monolayer is assumed to have a thickness of 0.335 nm, equal to the out of plane extension of the π-orbitals.[36] The chaotically oriented emitting dipoles are located on a plane in the middle of the graphene layer. The propagation of the plane waves of the excitation light and the plane waves emitted by the oscillating dipoles is simulated by the transfer matrix method.[34, 35] The spectral dependencies of the refractive indices of graphene, Si, SiO2 and Al2O3 are taken from the literature.[37, 38] The refractive indices used in the calculations are shown in Table 1 for the most common wavelengths used as Raman excitation sources. The wavenumbers of the Si–Si and G-bands of the Raman signal were redshifted by 520 and 1580 cm−1, respectively. In all the calculations used in this article, we assumed that the angle of incidence of the excitation light is 60°. Note that the intensity of the signal at all frequencies is determined by the internal quantum efficiencies of the corresponding bands (see, for example, theory developed in Refs.[39, 40]) and optical effects such as multi-reflection and interference, as well as by the spectral sensitivity of the experimental setup. The calculation described here deals only with the optical part of the Raman intensity.

Table 1. Optical constants of the materials used in calculations

Substance	457 nm	488 nm	514 nm	633 nm
Si	4.61–0.14*i*	4.37–0.08*i*	4.23–0.06*i*	3.88–0.02*i*
Al_2O_3	1.671	1.688	1.665	1.659
SiO_2	1.465	1.463	1.462	1.457
Graphene	2.69–1.49*i*	2.68–1.51*i*	2.68–1.54*i*	2.74–1.70*i*

In addition to the calculation of the intensity of Raman scattering, it is important to evaluate the visibility of the graphene layer under white light illumination. In order to characterize the visibility of graphene layer, we calculate the total color difference between the structure with graphene and the substrate.[13] We begin by calculating the X, Y and Z tristimulus components using color matching equations, introduced by the International Commission on Illumination (CIE)[41]:

$$\begin{cases} X = \dfrac{1}{N}\int_{vis} S(\lambda)R(\lambda)x(\lambda)d\lambda \\ Y = \dfrac{1}{N}\int_{vis} S(\lambda)R(\lambda)y(\lambda)d\lambda \\ Z = \dfrac{1}{N}\int_{vis} S(\lambda)R(\lambda)z(\lambda)d\lambda \end{cases}$$

Here, S(λ) is the light source spectrum, R(λ) is the reflectance spectrum of the structure, x(λ), y(λ) and z(λ) are the standard color matching functions. The color matching functions are a numerical description of the chromatic response of the human eye.[41] 1/N is the normalization factor and is usually chosen as inline image. Then, we have to move from CIE XYZ color space to CIE Lab color space[13]:

$$\begin{cases} L = \begin{cases} 116(Y/Y_0)^{1/3} - 16 & (Y/Y_0 > 0.008856) \\ 903.3Y/Y0 & (Y/Y_0 \le 0.008856) \end{cases} \\ a = \begin{cases} 500\left[(X/X_0)^{1/3} - (Y/Y_0)^{1/3}\right] & (X/X_0 > 0.008856) \\ 3893.5(X/X_0 - Y/Y_0) & (X/X_0 \le 0.008856) \end{cases} \\ b = \begin{cases} 200\left[(Y/Y_0)^{1/3} - (Z/Z_0)^{1/3}\right] & (Z/Z_0 > 0.008856) \\ 1557.4(Y/Y_0 - Z/Z_0) & (Z/Z_0 \le 0.008856) \end{cases} \end{cases}$$

where the parameters (X0,Y0,Z0) are called the white point of the CIE standard light source. In this work, we used D65 as a standard white light source. Knowledge of the psychological lightness, L, and the psychological chroma, tita and b, enables us to calculate the total color difference:

$$\Delta E = \sqrt{(\Delta L)^2 + (\Delta a)^2 + (\Delta b)^2},$$

which is the final image contrast between the graphene and the substrate.

Results and discussions

In order to investigate how the excitation wavelength influences the optimal thickness of the buffer layer, we calculated the intensity of the G-band of the Raman signal as a function of λexc and hbuf for SiO2 and Al2O3 buffer layers. The results of these calculations are shown in Fig. 2. The shaded vertical stripes in Figs. 2a and 2b denote buffer layer thicknesses providing a total color difference greater than 2, a value sufficient for optical visibility of graphene.

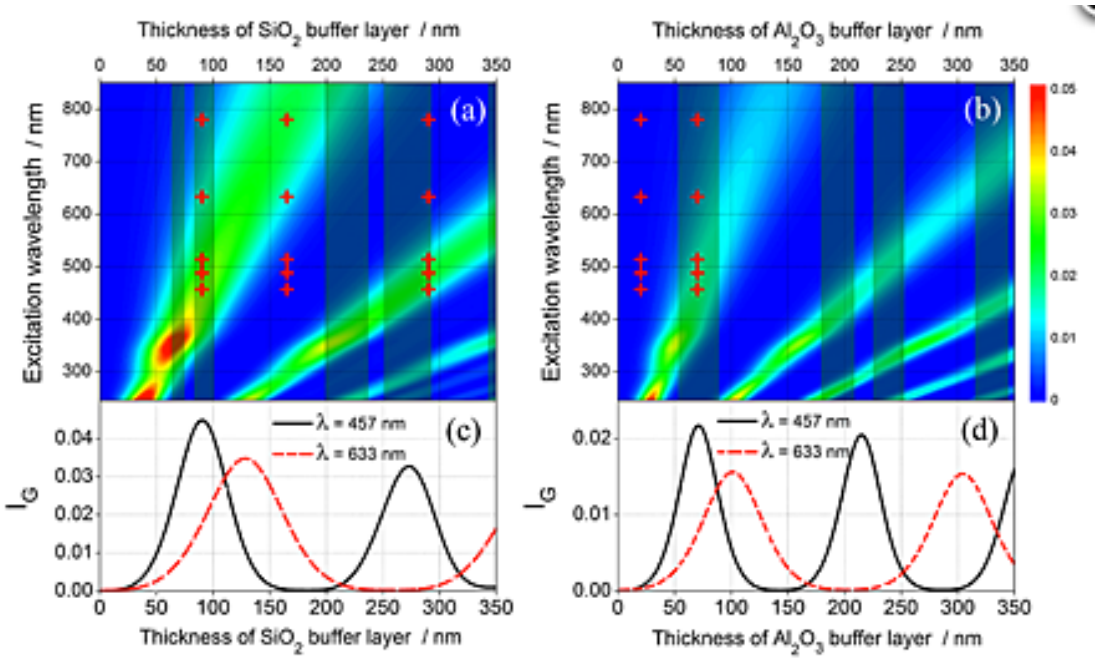

Figure 2. Intensity of the G-band of the Raman spectrum from samples with graphene layers as a two-dimensional function of the a) SiO2 and b) Al2O3 buffer layer thicknesses and excitation wavelength. Also shown are plots of IG and hdielec for c) SiO2 and d) Al2O3 using 457 nm (solid line) and 633 nm (dashed line) excitation. The selected most common laser wavelengths corresponding to extreme values of thicknesses of both type of buffer layers are shown by red crosses. The buffer layer thicknesses providing the highest optical contrast for each specific wavelength are denoted by black lines. The color scale on the right shows the Raman intensity in arbitrary units. This figure is available in colour online at wileyonlinelibrary.com/journal/jrs

Figure 2a shows that the maximal G-band intensity is achieved for UV excitation at wavelengths of 248 and 355 nm for SiO2 layer thickness of 43 and 71 nm, respectively. For an Al2O3 layer (see Fig. 2b), the maximum of the G-peak intensity appears at inline image nm and at λexc =350 nm. In addition, from the maps, particularly that for the SiO2 buffer layer, the region corresponding to an

intense G-peak is significantly wider for smaller thickness values. This enables a reasonable enhancement of the G-peak for most of the UV and visible excitation lines for an SiO2 layer thickness of 90 nm (shown by the red crosses in Fig. 2a). This is in good agreement with results from the literature.[17, 19] The second and third regions of enhanced G-peak intensity from Fig. 2a are significantly tilted with respect to the first region. These two regions are also almost half as wide as that discussed earlier. Selection options for excitation lines for the Raman investigation of samples with a specific thickness are limited to those identified by red crosses for inline image nm, for example. In this case, the strongest enhancement of the G-peak is obtained for an excitation wavelength of 457 nm, while for the red laser lines at 633 and 785 nm, only a minimal enhancement of the G-peak will be observed. This again corresponds with published data on the weak Raman signal observed using 633 nm excitation from a single graphene layer exfoliated onto a ~ 300 nm thick SiO2 buffer layer.[22, 42] It is worth noting that the results on reasonable enhancement of G-band intensity, demonstrated in Fig. 2a for UV excitation, are supported by experimental data obtained in Ref.[43] for graphene on 308 nm thick SiO2 buffer layer for 325 nm laser line.

In contrast, the opposite behavior can be expected, for example, for the SiO2 buffer layer with a thickness of 165 nm (shown by red crosses in Fig. 2a). In this case, an enhancement of G-peak can be expected only for the 633 and 785 nm excitation lines. For Al2O3, a similar situation is seen in Fig. 2b for 120 nm thick layer. In order to see the enhancement factor more clearly, Figs. 2c and 2d demonstrate the dependence of the intensity of the G-peak on the buffer layer thickness for 457 and 633 nm excitations. From these figures, we conclude that for 457 nm excitation line, for example, we can expect a significant enhancement of G-peak intensity for thicknesses of 90 and 290 nm and close to minimal enhancement for a 165 nm thick SiO2 buffer layer. For an Al2O3 buffer layer, minimal G-peak enhancement can be expected at thicknesses of ~ 10–20 nm and maximal enhancement at ~ 70 nm using a 457 nm excitation wavelength.

Based on this analysis, the thicknesses of SiO2 and Al2O3 buffer layers corresponding to the extreme cases shown in Fig. 2 were selected for experimental verification of these theoretical results, as described below.

Raman spectra of the sample investigated with a graphene layer are shown in Fig. 3 for 514 nm excitation line. The most prominent spectral features corresponding to graphene are the G-band at 1582 cm−1 and the 2D-band at 2685 cm−1. The G-peak originates from the in-plane vibrational phonon mode E2g at the Brillouin zone center and is associated with first order Raman scattering. The 2D-band is associated with second-order Raman scattering. From the shape and spectral position of the 2D-peak, we can distinguish single-layer graphene from the bulk graphite. For the single-layer graphene, the 2D-band is a single sharp Lorentzian peak, with a peak position below 2750 cm−1 and a line-

width of 30–40 cm−1 in contrast to the two-, or multi-component, peak that appeared for the FLG and bulk graphite.[10] In our case, the 2D-band consists of a single peak, with a line-width of 30–37 cm−1, corresponding to a single graphene layer. Raman spectra, shown in Fig. 3, are normalized to the intensity of the 2D-band to allow for convenient plotting. For both types of a buffer layer, the G-peak is revealed at ~ 1582 cm−1. The observed in Ref.[11] shift of G-band by ~ 5 cm−1 to the low wavenumbers for graphene on sapphire substrate was not obtained for our samples due to the amorphous nature of Al2O3 layer.

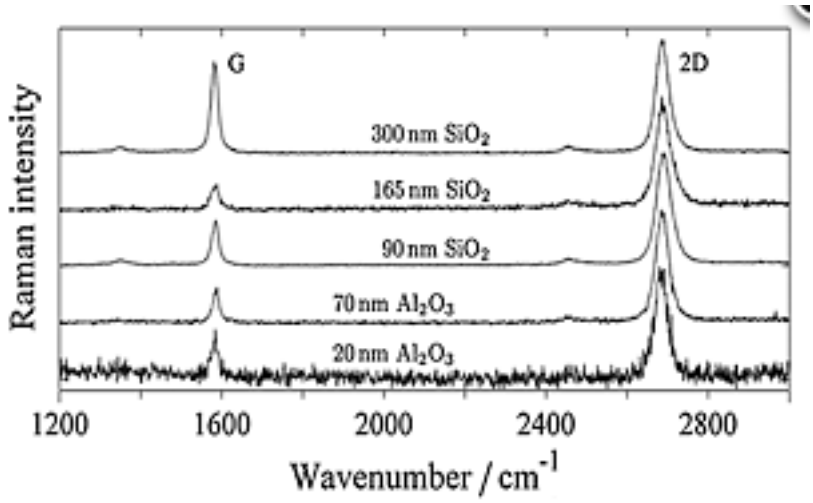

Figure 3. Raman spectra of graphene layers separated from the Si substrate by different buffer layers. Excitation wavelength is 514 nm.

It can be clearly seen from the spectra presented that, for this excitation line, the intensity of the Raman spectra in the region of the G- and 2D-bands for a 20 nm Al2O3 layer is much smaller than that for the 70 nm buffer layer, as evidenced by the much lower signal-to-noise ratio for the former. A similar conclusion can be drawn from a comparison of Raman spectra for a graphene layer exfoliated onto 90, 165 and 290 nm SiO2 buffer layers. For a 165 nm thick SiO2 layer, the Raman spectrum again has a much lower signal-to noise ratio, indicating that the intensity of the original spectrum is lower than that for the 90 and 290 nm thick SiO2 layers, in accordance with the maps shown in Figs. 2a and 2b.

In order to allow comparison with the theoretical results described earlier, we plotted the Raman spectra of graphene on SiO2 layers of different thicknesses for all three of the samples investigated registered at two excitation wavelengths, namely 457 nm (Fig. 4a) and 633 nm (Fig. 4b). From Figs. 4a and 4b, the peak position of the G-peak remains almost unchanged, while the peak position of the 2D-band is shifted by nearly 100 cm−1 from inline image cm−1 (for 457 nm excitation) to inline image cm−1 (for 633 nm excitation) since we are probing different points in momentum space for the electronic and phonon dispersion at different excitation energies, or wavelengths.[10] We note that the peak position of 2D-band at 457 nm excitation is in accordance with experimental and

theoretical results reported in Ref.[43] on dependence of the 2D-band position on the excitation energy.

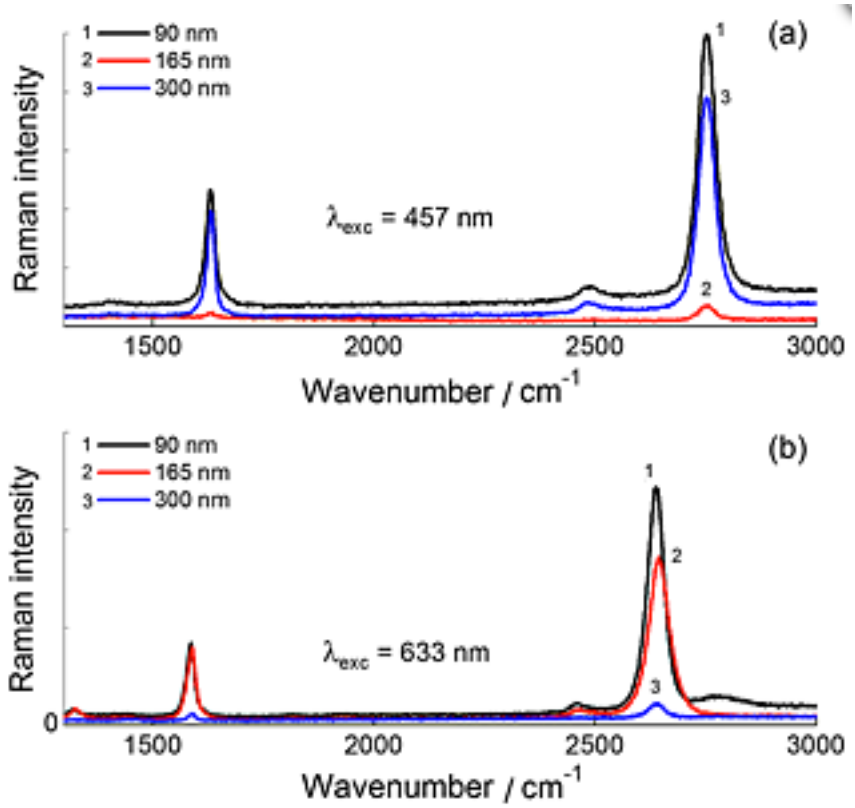

Figure 4. Raman spectra of graphene exfoliated onto a SiO2 buffer layer of various thicknesses (90 nm — black line (1), 165 nm — red line (2) and 290 nm — blue line (3)) for different excitation wavelengths: (a) 457 nm and (b) 633 nm. This figure is available in colour online at wileyonlinelibrary.com/journal/jrs

Figure 4a shows that for the 457 nm excitation line, the graphene spectrum for a 165 nm thick SiO2 layer has the lowest intensity, while the intensity of both bands (that is, the G and 2D) for the 90 and 290 nm thick buffer layers, are nearly 15 times higher. Also, the Raman intensity of graphene for the 290 nm thick buffer layer is slightly lower than that for the 90 nm thick buffer. This agrees with the results from the map of Fig. 2a. Figure 4b shows Raman spectra from the same samples using the 633 nm excitation line. Now, the graphene spectrum for the 290 nm thick buffer layer has the lowest intensity, while the intensity of the G-band and 2D-band is much higher for graphene on the 165 nm thick buffer, and only slightly lower for the 90 nm thick SiO2 layer. Again, this result is in excellent agreement with the data shown in Fig. 2a for these three samples using 633 nm excitation.

The intensities of the G-band which are obtained experimentally and those calculated by the oscillating dipoles method cannot be compared with each other directly because the Raman intensity observed depends on the experimental

conditions. In order to quantitatively compare the theoretical and experimental results, we calculate the ratio of the intensity of the G-band to the intensity of the Si band (at 520 cm−1), IG/ISi. The results of these calculations are shown for different excitation wavelengths in Figs. 5 and 6. As mentioned before, we have not made any assumptions regarding the internal quantum efficiencies of the Raman scattering at the frequencies of the G- or Si-bands. Therefore, the dependencies IG/ISi presented in Figs. 5 and 6, concern only the optical part of the Raman signal. In order to demonstrate how the optical effects influence the ratio IG/ISi, we normalized the experimental dependencies of IG/ISi to the corresponding theoretical ones. It can be seen from Figs. 5 and 6 that the ratio is a periodic function of the buffer layer thickness. The period of this function depends on the excitation wavelength and can be found from the two nearest Fabry-Perot resonances which appear during the propagation of the excitation light through the buffer layer: inline image, where λ is the excitation wavelength, n is the refractive index of the buffer layer and f is the angle made by the light propagating in the buffer layer. The maximal Raman intensities of the samples are up to 50 times higher than the minimal ones. The experimentally obtained data are in agreement with the theoretical curves. The intensities of the Raman scattering of graphene for the SiO2 buffer layer are approximately 1.5 times higher than those for the Al2O3 layer. From Figs. 5 and 6, it follows that the intensity of the G-band of Raman scattering for 457 nm excitation is approximately one order of magnitude higher than that for 633 nm excitation. We conclude that the use of the 457 nm excitation line is more preferable than, for example, a 633 nm excitation. We would like to emphasize that this conclusion was drawn without any assumptions being made about the internal efficiencies of different Raman scattering bands.

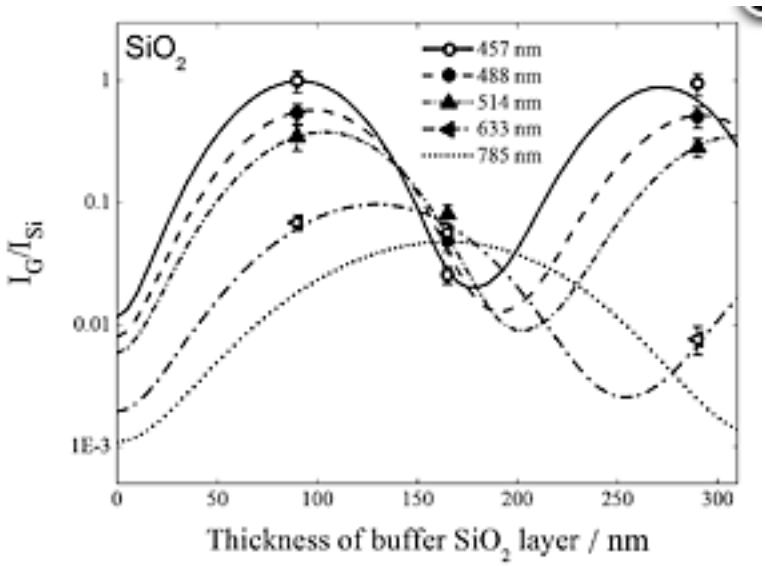

Figure 5. Calculated (lines) and experimental (symbols) values of the ratio IG/ISi as a function of SiO2 buffer layer thickness for different excitation wavelengths. The experimental data are normalized to the corresponding theoretical data.

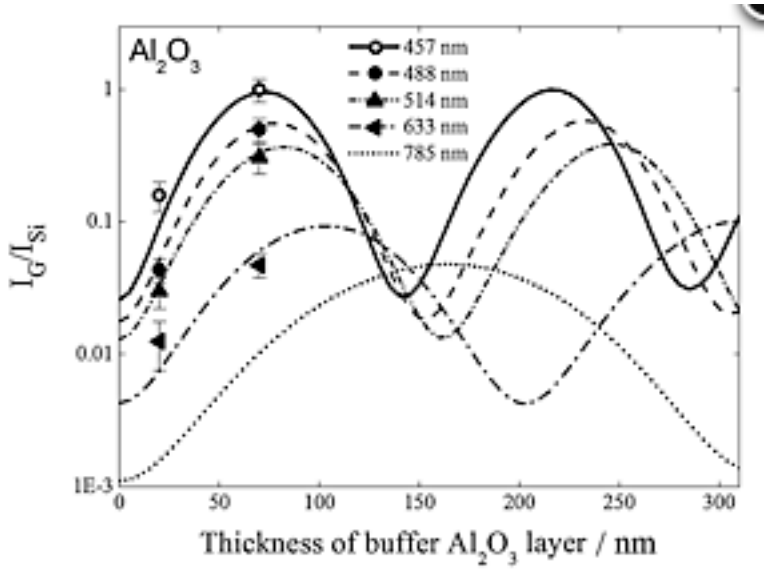

Figure 6. Calculated (lines) and experimental (symbols) values of the ratio IG/ISi as a function of Al2O3 buffer layer thickness for different excitation wavelengths. The experimental data are normalized to the corresponding theoretical data.

In order to evaluate the influence of the buffer layer properties on the Raman intensity of the G-peak, we calculated the Raman intensity as a two-dimensional function of thickness and the refractive index of the buffer layer. Figure 7 shows the results of this calculation for an excitation wavelength of 457 nm. It depicts the region where the intensity of the G-band exceeds 25% of the highest Raman intensity. In contrast to Figs. 5 and 6, the intensities of the G-band of Raman scattering, which are shown in Fig. 7, are not normalized by dividing by the intensity of the Si band. Similar maps can be obtained for other excitation wavelengths. In addition to the high Raman intensity, Fig. 7 shows regions where the total color difference exceeds 2, sufficient for optical visibility of graphene. From Fig. 7, the regions of the high Raman intensity and the high optical contrast do not always coincide. The intersections of these regions correspond to the optimal substrate as indicated by our experimental investigation of graphene.

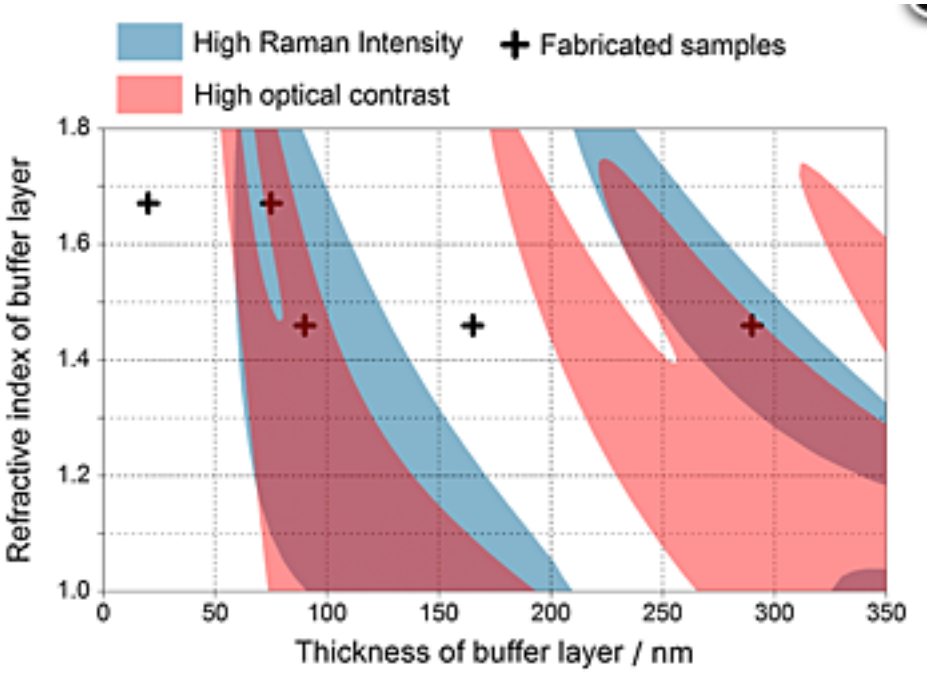

Figure 7. Regions of high Raman intensity (> 0.25Imax) and high total color difference (ΔE > 2). This figure is available in colour online at wileyonlinelibrary.com/journal/jrs

For the sake of completeness, the theoretical simulations of the optical contrast of graphene are verified experimentally for the samples investigated. Indeed, Fig. 8 demonstrates that single-layer graphene areas are clearly visible for buffer layers of 90 nm and 290 nm of SiO2 and 70 nm of Al2O3 whereas those samples with 165 nm of SiO2 and 20 nm of Al2O3 are characterized by a low optical contrast.

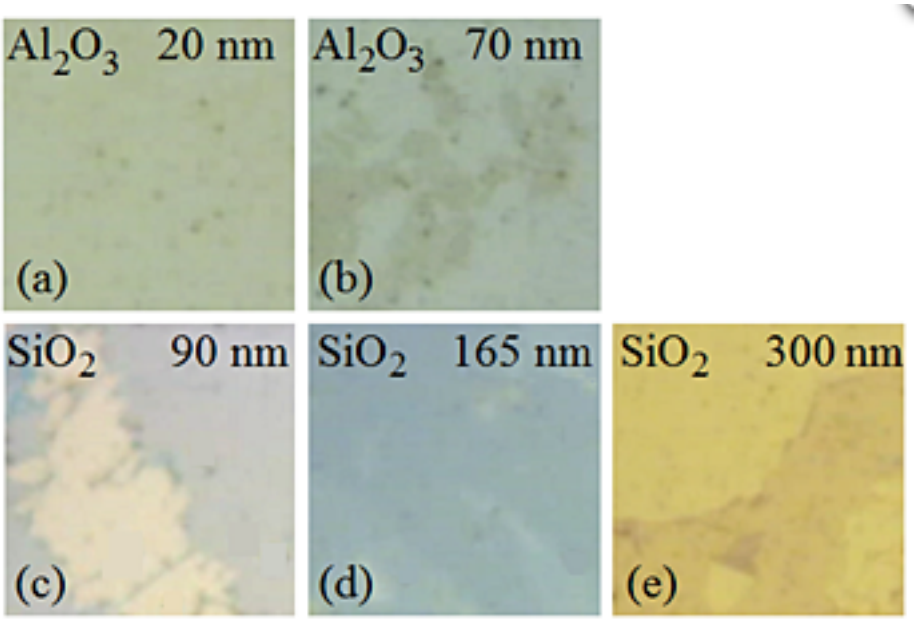

Figure 8. (Color online) Optical images of the samples with graphene layers (a), (b) with Al2O3 substrate and (c)–(e) SiO2 substrate.

Conclusions

In conclusion, we have produced a simultaneous presentation of Raman intensity of G-band and optical contrast maps for a single layer of graphene, as a function of refractive index and buffer layer thickness. This presentation enables selection of the buffer layer material in order to optimize Raman and optical microscopy imaging. The advantages of this technique, demonstrated at an excitation wavelength of 457 nm, are confirmed experimentally for two dielectric materials viz. SiO2 and Al2O3 with different refractive indexes and thicknesses. It has been also shown that for an SiO2 buffer layer thickness in the range of 150–160 nm, substantial enhancement of the G-band intensity from a single graphene layer can be achieved, even at longer excitation wavelengths of 633 and 785 nm.

Acknowledgements

The authors would like to thank Joanna Wasyluk for useful discussions. S. A. D thanks IRCSET and Trinity College Dublin for financial support. D. McNeill and Shahjahan Newaz Ali Murad are gratefully acknowledged for performing the ALD of Al2O3 onto a silicon substrate. This work was supported in part by the RFBR (Grants 12-02-01263 and 12-02-00938) and the Ministry of Education and Science of the Russian Federation (Projects 11.519.11.3020, 11.519.11.3026, 14.B37.21.0741 and 14.B37.21.1954).

We assume that an electromagnetic wave emitted by one plane does not interact with other planes or waves.

References

A. K. Geim, K. S. Novoselov, Nat. Mat. 2007, 6, 183.

P. Gava, M. Lazzeri, A. M. Saitta, F. Mauri, Phys. Rev. B 2009, 79, 165431.

X. Li, Y. Zhu, W. Cai, M. Borysiak, B. Han, D. Chen, R. D. Piner, L. Colombo, R. S. Ruoff, Nano Lett. 2009, 9, 4359.

I. Khrapach, F. Withers, T. H. Bointon, D. K. Polyushkin, W. L. Barnes, S. Russo, M. F. Craciun, Adv. Mat. 2012, 24, 2844.

C. Mattevi, H. Kim, M. Chhowalla, J. Mater. Chem. 2010, 21, 3324.

Q. Yu, J. Lian, S. Siriponglert, H. Li, Y. Chen, S. S. Pei, Appl. Phys. Lett. 2008, 93, 113 103.

K. S. Kim, Y. Zhao, H. Jang, S. Y. Lee, J. M. Kim, K. S. Kim, J. H. Ahn, P. Kim, J. Y. Choi, B. H. Hong, Nature 2009, 457, 706.

X. Li, W. Cai, J. An, S. Kim, J. Nah, D. Yang, R. Piner, A. Velamakanni, I. Jung, E. Tutuc et al., Science 2009, 324, 1312.

W. Liu, C. H. Chung, C. Q. Miao, Y. J. Wang, B. Y. Li, L. Y. Ruan, K. Patel, Y. J. Park, J. Woo, Y. H. Xie, Thin Solid Films 2010, 518, S128.

L. M. Malard, M. A. Pimenta, G. Dresselhaus, M. S. Dresselhaus, Phys. Rep. 2009, 473, 51.

I. Calizo, W. Bao, F. Miao, C. N. Lau, A. A. Balandin, Appl. Phys. Lett. 2007, 91, 201 904.

P. Blake, E. Hill, A. H. C. Neto, K. S. Novoselov, D. Jiang, R. Yang, T. J. Booth, A. K. Geim, Appl. Phys. Lett. 2007, 91, 063124.

L. Gao, W. Ren, F. Li, H. M. Cheng, ACS Nano 2008, 2, 1625.

O. Albrektsen, R. L. Eriksen, S. M. Novikov, D. Schall, M. Karl, S. I. Bozhevolnyi, A. C. Simonsen, J. Appl. Phys. 2012, 111, 064 305.

C. Kontis, M. R. Mueller, C. Kuechenmeister, K. T. Kallis, J. Knoch, Appl. Opt. 2012, 51, 385.

K. Peters, N. Gayer, A. Graf, V. Paulava, U. Wurstbauer, W. Hansen, Appl. Phys. Lett. 2011, 99, 191 912.

A. Gupta, G. Chen, P. Joshi, S. Tadigadapa, P. C. Eklund, Nano Lett. 2006, 6, 2667.

F. Herziger, P. May, J. Maultzsch, Phys. Rev. B 2012, 85, 235447.

CrossRef,

CAS,

Y. K. Koh, M. H. Bae, D. G. Cahill, E. Pop, ACS Nano 2011, 5, 269.

D. Graf, F. Molitor, K. Ensslin, C. Stampfer, A. Jungen, C. Hierold, L. Wirtz, Nano Lett. 2007, 7, 238.

P. H. Tan, W. P. Han, W. J. Zhao, Z. H. Wu, K. Chang, H. Wang, Y. F. Wang, N. Bonini, N. Marzari, N. Pugno, Nat. Mater. 2012, 11, 294.

A. C. Ferrari, J. C. Meyer, V. Scardaci, C. Casiraghi, M. Lazzeri, F. Mauri, S. Piscanec, D. Jiang, K. S. Novoselov, S. Roth, Phys. Rev. Lett. 2006, 97, 187401.

D. Yoon, H. Moon, Y. W. Son, J. S. Choi, B. H. Park, Y. H. Cha, Y. Kim, H. Cheong, Phys. Rev. B 2009, 80, 125422.

D. Yoon, H. Moon, Y. W. Son, G. Samsonidze, B. Park, J. B. Kim, Y. P. Lee, H. Cheong, Nano Lett. 2008, 8, 4270.

J. Yan, Y. Zhang, P. Kim, A. Pinczuk, Phys. Rev. Lett. 2007, 98, 166802.

S. Pisana, M. Lazzeri, C. Casiraghi, K. S. Novoselov, A. Geim, A. Ferrari, F. Mauri, Nat. Mat. 2007, 6,198.

S. Berciaud, S. Ryu, L. E. Brus, T. F. Heinz, Nano Lett. 2008, 9, 346.

Y. Y. Wang, Z. H. Ni, Z. X. Shen, H. M. Wang, Y. H. Wu, Appl. Phys. Lett. 2008, 92, 043121.

R. J. Walters, J. Kalkman, A. Polman, H. A. Atwater, M. J. A. De Dood, Phys. Rev. B 2006, 73, 132302.

K. A. Neyts, J. Opt. Soc. Am. A 1998, 15, 962.

R. Meerheim, M. Furno, S. Hofmann, B. Lüssem, K. Leo, Appl. Phys. Lett. 2010, 97, 253305.

H. Benisty, R. Stanley, M. Mayer, J. Opt. Soc. Am. A 1998, 15, 1192.

C. E. Reed, J. Giergiel, J. C. Hemminger, S. Ushioda, Phys. Rev. B 1987, 36, 4990.

M. Born, E. Wolf, A. B. Bhatia, Principles of optics: electromagnetic theory of propagation, interference and diffraction of light, Cambridge Univ Pr, 1999.

P. Markoš, C. M. Soukoulis, Wave propagation: from electrons to photonic crystals and left-handed materials, Princeton Univ Pr, 2008.

L. Pauling, The Nature of the Chemical Bond, Cornell University Pr, 1960.

E. D. Palik, G. Ghosh, Handbook of optical constants of solids, Academic Pr, 1998.

J. W. Weber, V. E. Calado, M. C. M. Van de Sanden, Appl. Phys. Lett. 2010, 97, 091904.

D. M. Basko, Phys. Rev. B 2007, 76, 081405.

D. M. Basko, Phys. Rev. B 2008, 78, 125418.

S. Janos, Colorimetry: understanding the CIE system, John Wiley & Sons, New Jersey, 2007.

C. H. Lui, Z. Li, Z. Chen, P. V. Klimov, L. Brus, T. F. Heinz, Nano Lett. 2011, 11, 164.

I. Calizo, I. Bejenari, M. Rahman, G. Liu, A. A. Balandin, J. Appl. Phys. 2009, 106, 043 509.